The physical parameters, excitation and chemistry of the rim, jets and knots of the planetary nebula NGC 7009 [1]

Denise R. Gonçalves
Instituto de Astrofísica de Canarias,
E-38205 La Laguna, Tenerife, Spain
e-mail: denise@ll.iac.es

Romano L. M. Corradi
Isaac Newton Group of Telescopes,
Apartado de Correos 321, E-38700, Sta. Cruz de la Palma, Spain
e-mail: rcorradi@ing.iac.es

Antonio Mampaso
Instituto de Astrofísica de Canarias,
E-38205 La Laguna, Tenerife, Spain
e-mail: amr@ll.iac.es

Mario Perinotto
Dipartimento di Astronomia e Scienza dello Spazio, Università di Firenze,
Largo E. Fermi 5, 50125 Firenze, Italy
e-mail: mariop@arcetri.astro.it

ABSTRACT

We present long-slit optical spectra along the major axis of the planetary nebula NGC 7009. These data allow us to discuss the physical, excitation and chemical properties of all the morphological components of the nebula, including its remarkable systems of knots and jets. The main results of this analysis are the following: *i)* the electron temperature throughout the nebula is remarkably constant, T_e[O III] = 10 200 K; *ii)* the bright inner rim and inner pair of knots have similar densities of $N_e \sim 6000$ cm^{-3}, whereas a much lower density of $N_e \sim 1500$ cm^{-3} is derived for the outer knots as well as for the jets; *iii)* all the regions (rim, inner knots, jets and outer knots) are mainly radiatively excited; and *iv)* there are no clear abundance changes across the nebula for He, O, Ne, or S. There is a marginal evidence for an overabundance of nitrogen in the outer knots (ansae), but the inner ones (caps) and the rim have similar N/H values that are at variance with previous results. Our data are compared to the predictions of theoretical models, from which we conclude that the knots at the head of the jets are not matter accumulated during the jet expansion through the circumstellar medium, neither can their origin be explained by the proposed HD or MHD interacting-wind models for the formation of jets/ansae, since the densities as well as the main excitation mechanisms of the knots, disagree with model predictions.

Subject headings: planetary nebulae: individual (NGC 7009) - ISM: kinematics and dynamics - ISM: jets and outflows

1. Introduction

In addition to their large-scale structures, mainly identified in the forbidden [OIII] emission line, many planetary nebulae (PNe) have a number of smaller-scale structures which are instead more prominent in low-ionization lines, such as [N II], [O II] and [S II]. In a previous paper (Gonçalves, Corradi, & Mampaso 2001), we have used the acronymous LISs to identify these low-ionization structures. LISs appear with different morphological and kinematical properties in the form of pairs of knots, filaments, jets, or isolated features moving with supersonic velocities through the large-scale components in which they are located, or instead as structures with the above morphologies but with low velocities that do not differ substantially from that of the main nebula[2]. LISs can be easily seen in the imaging catalogues of Balick (1987), Schwarz, Corradi, & Melnick (1992), Manchado et al. (1996), Corradi et al. (1996) and Górny et al. (1999). For a detailed study concerning the morphological and kinematical classification of LISs in PNe, see Gonçalves et al. (2001).

A very interesting class of LISs are jets. These are highly collimated outflows (with aspect ratios varing between 3 and 20; López 1997), which are directed radially outward from the central star, appear in opposite symmetrical pairs, and move with velocities substantially larger than those of the ambient gas that forms the main bodies of the nebulae. It should be noted in addition that jets are much more collimated than other bipolar outflows of PNe, i.e, more collimated than the lobes of a bipolar PN.

NGC 7009, the "Saturn Nebula", is a well studied elliptical PN, which possesses a jet-like system as well as two pairs of low-ionization knots along its major axis. A number of previous studies showed that high-excitation lines dominate the inner regions along the minor axis, while the low-excitation ones are enhanced at the ends of the major axis. The ionization structure is further enriched by the fact that the low-excitation region present strong variations in excitation level and clumpiness. NGC 7009 was classified as an oxygen-rich PN (Hyung & Aller 1995), with an O/C ratio exceeding 1, and anomalous N, O, and C abundances (Baker 1983; Balick et al. 1994, Hyung & Aller 1995). Its central star is an H-rich O-type star, with effective temperature of 82 000 K (Méndez, Kudritzki, & Herrero 1992; Kingsburgh & Barlow 1992). The kinematics of NGC 7009 was studied by Reay & Atherton (1985) and Balick, Preston & Icke (1987). The distance determinations of NGC 7009 vary from 0.5 to 2.3 kpc from various indirect methods (Acker et al. 1992; Cahn, Kaler & Stanghellini 1992; Maciel 1995).

According to the theoretical models for the formation of jets and of the pairs of knots that are often found at their tips (Soker 1990; García-Segura 1997; García-Segura et al. 1999; García-Segura & López 2000; Steffen, López, & Lim 2001; Gardiner & Frank 2001; Blackman, Frank, & Welch 2001), a significant density contrast between the jet itself and the knots at its tip is expected. This is a quantity that can in principle be determined by optical spectroscopy.

In addition, previous observational work suggests that the LISs of NGC 7009 and other PNe have higher abundances of nitrogen than their main bodies (see Balick et al. 1994 and references therein). These authors proposed that such an overabundance might indicate that the knots of NGC 7009 were ejected at a different epoch than the main body of the nebula, when the stellar surface was enriched of these elements due to the drastic changes of nitrogen in AGB stars and some dredge-up episode, or that the knots come from chemically peculiar regions in the stellar surface or its interior.

In this paper, we test the above two issues by obtaining spectroscopic data for NGC 7009, deriving its physical and chemical properties, and finally showing that neither a density contrast between the jets and knots is found, nor are their abundances strongly enhanced compared to the rest of the nebula. In the following sections, we first describe the data, their reduction and the various morphological/kinematical structures of the nebulae (Sections 2 and 3). Then we proceed with

[1] Based on observations obtained at the 2.5 m Isaac Newton Telescope (INT) of the European Northern Observatory, and with the NASA/ESA *Hubble Space Telescope*, obtained at the Space Telescope Science Institute, which is operated by AURA for NASA under contract NAS5-26555.

[2] The fast, low-ionization emission regions, FLIERs (Balick et al. 1993) and bipolar, rotating, episodic jets, BRETs (López, Vázquez, & Rodríguez 1995) are particular types of LISs, i.e., high-velocity knots and jets.

the analysis of the PN spectra in terms of physical, excitation and chemical parameters (Section 4) and, finally, we discuss the implication of the present results for the formation of the LISs of NGC 7009 and give our conclusions, in Sections 5 and 6.

2. Observations and Data Reduction

Spectra of NGC 7009 (PN G037.7-34.5) were obtained on 2001 August 29 at the 2.5 m Isaac Newton Telescope (INT) at the Observatorio del Roque de los Muchachos (European Northern Observatory, La Palma, Spain), using the Intermediate Dispersion Spectrograph (IDS). The IDS was used with the 235 mm camera and the R300V grating, providing a spectral coverage from 3650 Å to 7000 Å with a spectral reciprocal dispersion of 3.3 Å pix^{-1}. The spatial scale of the instrument was $0''.70$ pix^{-1} with the TEK5 CCD. Seeing varied from $0''.9$ to $1''.1$. The slit width and length were $1.5''$ and $4'$, respectively. The slit was positioned through the center of the nebula at P.A. = 79°, and the exposure times were 3×30 s, 3 × 120 s, and 3 × 600 s.

During the night, bias frames, twilight and tungsten flat-field exposures, wavelength calibrations and exposures of standard stars (BD+332642, Cyg OB2#9, HD19445, and BD+254655) were obtained. Spectra were reduced following the IRAF instructions for long-slit spectra, being bias-subtracted, flat-fielded, combined in order to improve the signal-to-noise ratio and eliminate cosmic rays, wavelength calibrated, and sky-subtracted. Finally, they were flux-calibrated using the above-mentioned standard stars and the mean atmospheric extinction curve for La Palma.

We also retrieved *HST* [N II] and [O III] archive images of NGC 7009 obtained on 1996 April 28, and on 2000 April 7, respectively, with the WFPC2 camera in the F658N and F502N filters, with total exposure times of 1200 s and 320 s.

3. The morphological and kinematical components of NGC 7009: previous works

The *HST* [O III] and [N II] images of NGC 7009 are shown in Figure 1. The nebula consists of several components. The brightest one is the elliptical inner shell (*rim*) roughly elongated in the EW direction, where it extends out to $\pm 13''$ from the center. The inner portions of the rim cut by our spectroscopic slit are indicated in Figure 1 (bottom) by the labels R_1 and R_2.

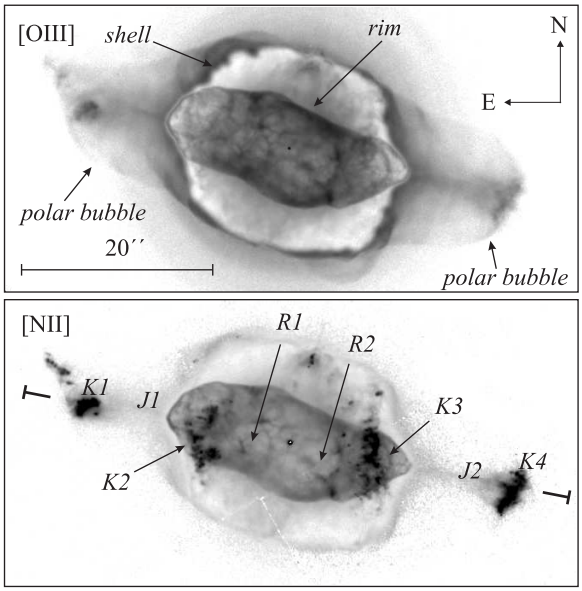

Fig. 1.— The *HST* [O III] and [N II] images of NGC 7009 on a logarithmic intensity scale. Slit position is indicated by short lines (P.A. = 79°), while labels mark the position of the several structures, where "K", "J" and "R" stand for "knot", "jetlike", and "rim", respectively. Extensions of the selected structures with respect to the central star are: from $-26.6''$ to $-21.7''$, K_1; from $-20.3''$ to $-16.1''$, J_1; from $-14.7''$ to $-6.3''$, K_2; from $-4.9''$ to $-1.4''$, R_1; from $2.1''$ to $3.5''$; R_2; from $4.9''$ to $14.0''$, K_3; from $17.5''$ to $22.4''$, J_2; and from $23.8''$ to $28.7''$, K_4.

Surrounding the rim, a fainter elliptical outer shell (*shell*) that shares its main axis with the rim is also visible in the *HST* images. In [O III], at fainter intensity levels the shell shows two "polar" bubbles. Inside these bubbles, collimated LISs are clearly seen in the [N II] images. These are composed of a "pencil" of emission (the *jetlike* structures, labeled J_1 and J_2) that connects the inner rim with two *outer knots* (K_1 and K_4). The [N II] image also shows another pair of microstructures, which appear as "compact groups of bright knots" that we call the *inner knots* (K_2 and K_3). The extension of all features is given in the caption of

Figure 1.

The rim of NGC 7009 is likely to be formed by the interaction between the fast post-AGB and the slow AGB winds (Kwok, Purton, & Fitzgerald 1978; Frank & Mellema 1994; Mellema & Frank 1995; Zhang & Kwok 1998, Schönberner 2002). The cavity delimited by the rim is filled with a hot ($T = 1.8 \times 10^6$ K) gas emitting thermal X-rays and its size is in agreement with that of the optical rim (Guerrero, Gruendl, & Chu, 2002) providing a direct proof for the shocked fast stellar wind in the interacting winds scenario. The formation of the shell has been ascribed to the action of the photoionization front on the AGB matter not yet reached by the shock produced by the fast wind (e.g., Schönberner 2002).

The origin and nature of the LISs in NGC 7009 are rather unclear at present. The inner and outer pairs of knots have been studied by many authors (Reay & Atherton 1985; Balick et al. 1994; Hyung & Aller 1995; Lame & Pogge 1996; Balick et al. 1998), who often called them *caps* and *ansae*, respectively. Reay & Atherton (1985) have studied the kinematics of the inner and outer knots in the [O I] 6300 Å line using Fabry–Perot data. They derived an expansion velocity for the inner knots of $\pm 38\,\mathrm{km\,s^{-1}}$ with an inclination with respect to the line of sight $i \cong 51°$, and a velocity of ± 60 $\mathrm{km\,s^{-1}}$ with $i \cong 84°$ for the outer pair. Note that the determination of the deprojected velocities and inclination angles by Reay & Atherton (1985) is mainly based on the proper motion measurements of Liller (1965), as the velocity in the plane of the sky appears one order of magnitude larger than the Doppler shift. We have estimated the separation of the outer knots in the [N II] *HST* image taken in 1996, finding $\sim$50.8 $\pm$ 0.5 arcsec, the uncertainty depending on the highly irregular morphology of these knots that makes it difficult to define a centroid. This is clearly not consistent with the extrapolation of Liller's measurements (separation of 48 arcsec in 1965 and apparent expansion of 1.6 arcsec per century for each knot), making the velocity and inclination figures of Reay & Atherton (1985) quite uncertain. Their analysis also depends on the distance adopted, which is poorly known, as mentioned in the introduction.

No velocity information is available from the literature for the jetlike structures connecting the rim to the outer knots. If we assume a continuity between the velocity of the outer knots and these jetlike structures, then the latter might be real supersonic jets. A more detailed study of the kinematics of NGC 7009, and in particular of the faint "pencil" and large-scale structures surrounding it (shell and polar bubbles), is clearly needed to understand its nature better.

4. Data Analysis

Line intensities were mainly measured from the deep spectrum with 3×600 s exposure time. The shorter-exposure spectra were used to measure the bright Hβ, [O III], Hα, and [N II] lines that are saturated in the deep spectra. Measurements are given in Table 1, which lists the wavelength of the line identification and the corresponding ion (column 1), the line fluxes measured for the different spatial regions selected (columns 2 to 9, as defined in Fig. 1 and Section 3), and the flux integrated along the slit for the whole nebula, labeled as NEB (column 10). All fluxes are normalized to I(Hβ) = 100 in each of the regions considered.

Errors in the fluxes were calculated taking into account the statistical error in the measurement of the fluxes, as well as systematic errors of the flux calibrations, background determination, and sky subtraction. Table 2 gives the estimated accuracy of the measured fluxes for a range of line fluxes (relative to Hβ) in each of the selected regions. Absolute Hβ fluxes integrated along the slit in each region are also given in Table 2.

4.1. Extinction

Fluxes were extinction-corrected by using $c_{\mathrm{H}\beta}$=0.16± 0.01 (the logarithmic ratio between observed and dereddened Hβ fluxes), determined from the Hα/Hβ ratio in the brightest regions of the nebula ($\mathrm{R_1}$ and $\mathrm{R_2}$). For the derivation of $c_{\mathrm{H}\beta}$, we assumed $T_{\mathrm{e}} = 10^4$ K and $n_{\mathrm{e}} = 10^4$ cm^{-3}, appropriate for the values that we have computed in the rim (Section 4.2). Theoretical Balmer line ratios from Osterbrock (1989) and the reddening law of Cardelli, Clayton, & Mathis (1989) were used. Our derived value is in fair agreement with the average value (0.15) reported by other authors: $c_{\mathrm{H}\beta} = 0.08 \pm 0.03$ (Hyung & Aller 1995); $c_{\mathrm{H}\beta} = 0.24 \pm 0.04$ (Lame & Pogge 1996); $c_{\mathrm{H}\beta} =$ 0.20 (Liu et al. 1995); $c_{\mathrm{H}\beta} = 0.10$ (Rubin et al. 2002).

Note that we applied $c_{H\beta} = 0.16$ for the fluxes of all the different zones under analysis, because of the highest S/N ratio of the rim, thus avoiding the larger errors in the measured Balmer line ratios of the fainter zones. This assumption of a constant extinction throughout the nebula is supported by the work of Bohigas, López, & Aguilar (1994), who reported that the $c_{H\beta}$ for the different structures of NGC 7009 are always lower than 0.28, implying small corrections to the observed fluxes.

4.2. Densities and Temperatures

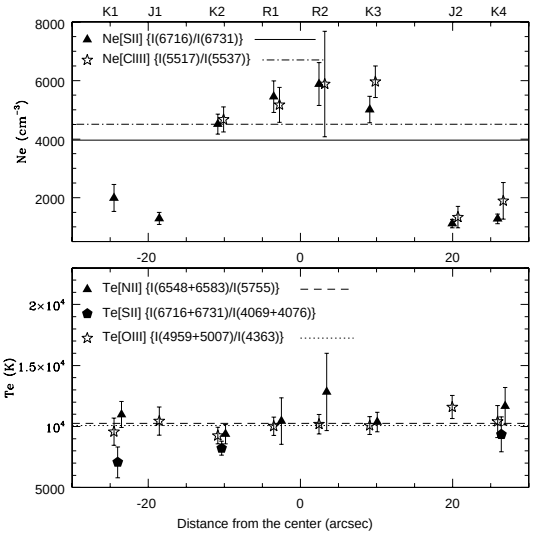

Fig. 2.— Electron densities and temperatures determined with different line ratios as a function of the distance from the center of NGC 7009. The positions of the various features are marked in the uppermost part of the plot (see Figure 1). Symbols are plotted slightly displaced in distance in order to avoid overlapping. The horizontal lines in both plots give the value of each density/temperature estimate for the entire nebula: N_e[S II](NEB) = 4000 ± 300 cm^{-3} N_e[Cl III](NEB) = 4500 ± 400 cm^{-3}; T_e[O III](NEB) = 10 100 ±7 00 K, and T_e[N II](NEB) = 10 300 ± 800 K.

As described above, eight different regions were selected in the spectrum of NGC 7009 (see also Figure 1). The extinction-corrected fluxes were then used in order to obtain the densities and temperatures for each of the regions that are plotted in Figure 2. These physical parameters were obtained using the *nebular* package of IRAF (Shaw & Dufour 1995), based on the five-level atom program (De Robertis, Dufour, & Hunt 1987) to derive the physical conditions in a low-density nebular gas, including diagnostics for a large number of ions and emission lines.

To estimate densities, we assumed an electron temperature of 10^4 K (see below). In most positions, we were able to measure the densities from both the [S II] 6716 Å/6731 Å and [Cl III] 5517 Å/5537 Å line ratios. These provide a simultaneous estimate of densities in low-ionization ([S II]) and higher ionization ([Cl III]) regions. In general, we found a good agreement between the results from these two density estimators for most of the structures (see Table 1 and Figure 2). Using the total flux integrated along the slit, we obtain N_e[Cl III]/N_e[S II] ≅ 1.13; the horizontal dashed-dashed line in Figure 2 indicates the N_e[Cl III] overall value, while the continuous line shows the corresponding N_e[S II] overall density.

Figure 2 clearly shows that the densities of the outermost knots are very similar to those of the jets connecting them to the edge of the inner rim, with $N_e(K_1)$ = 1900 ± 500 cm^{-3} and $N_e(J_1)$= 1300±200 cm^{-3} and, on the opposite side, $N_e(K_4)$ = 1300 ± 200 cm^{-3} and $N_e(J_2)$ = 1300 ± 500 cm^{-3}. On the other hand, the inner pair of knots have higher electron densities, namely $N_e(K_2)$ = 4500 ± 400 cm^{-3} and $N_e(K_3)$ = 5000 ± 500 cm^{-3}, and similar to those of the rim ($N_e(R_1)$= 5500 ± 600 cm^{-3} and $N_e(R_2)$ = 5900 ± 800 cm^{-3}).

As for the densities, the temperature estimators used are appropriate for zones of low- and high-excitation. We used the following line ratios: I(4959 Å + 5007 Å)/I(4363 Å) for T_e[O III]; I(6548 Å + 6583 Å)/I(5755 Å) for T_e[N II]; and I(6716 Å/6731 Å)/I(4069 Å + 4076 Å) for T_e[S II]. The general trend of temperatures (Figure 2, bottom) is that, within the errors, they are constant throughout the nebula, having an average value of T_e[O III] = 10 200 K and T_e[N II] = 11 100 K. In spite of a small discrepancy of T_e[S II] at the position of R_2, the temperature is remarkably constant across this nebula.

There are a number of papers that discuss the physical properties of NGC 7009 (Rubin et al. 2002; Hyung & Aller 1995; Bohigas et al. 1994;

Balick et al. 1994). In general, there is good overall agreement between our temperature determinations and previous ones. A more detailed zone-by-zone comparison can be made with some of these papers. Balick et al. (1994) studied the west rim, cap, and ansae. They found T_e[N II] and T_e[O III] of 10 000 K and 9400 K, respectively, for the rim, 9600 K and 9600 K for the cap, and 8100 K and 11 500 K for the ansa. With the exception of T_e[N II] of that ansa, these figures are very similar to ours (see Table 1). From the six regions of the PN studied by Bohigas et al. (1994), two coincide with ours (those of the W and E ansae), and they found, for both structures, an [O III] temperature of 9800 K, again consistent, within the errors, with our measurements. The T_e[O III] determined from the *HST*/WFPC2 data by Rubin et al. (2002) is also consistent with the values we derived, since they found 9000 K $\leq T_e$[O III] $\leq$ 11 000 K. Their STIS long-slit results for temperature are limited to the 13 central arcseconds along the major axis. The average T_e[O III] for K_2, R_1, R_2, and K_3 are $\sim$10 300 K $\sim$10 700 K, $\sim$10 600 K, and $\sim$10 100 K, respectively, which are very similar to our figures in Table 1.

The above papers also report density estimates, whose agreement with our measurements is not, however, as good as for the electron temperatures. For instance, Balick et al. (1994) found Ne[S II] = 4900 cm^{-3}, 4100 cm^{-3}, and 1000 cm^{-3} for the western rim, cap, and ansae, respectively. They also found a large difference between the N_e[S II]/N_e[Cl III] ratio at the position of the W rim and cap, which was measured to be $\sim$3 and $\sim$0.4, respectively, while ours is $\sim$1.0 and $\sim$0.8 (in line with N_e[S II] $\approx$ N_e[Cl III] found by Copetti & Writzl 2002 for a large sample of PNe). Lame & Pogge (1996) found that the rim plus inner knots of NGC 7009 have densities as high as 8000 cm^{-3}, and that the rim without including K_2 and K_3 has a significantly lower density, $\sim$4000 cm^{-3}. There is also only moderate agreement between our densities and those of Bohigas et al. (1994), who obtained 2300 $\pm$ 600 cm^{-3} and 4300 $\pm$ 2700 cm^{-3} for the W and E ansae, respectively. The reason of the discrepancies between different authors might be the S/N ratio of the relevant lines, and the seeing. Note that our observations are, in general, much deeper and were obtained during better seeing conditions than the above studies, allowing a more precise definition of the spatial regions.

4.3. Excitation Properties

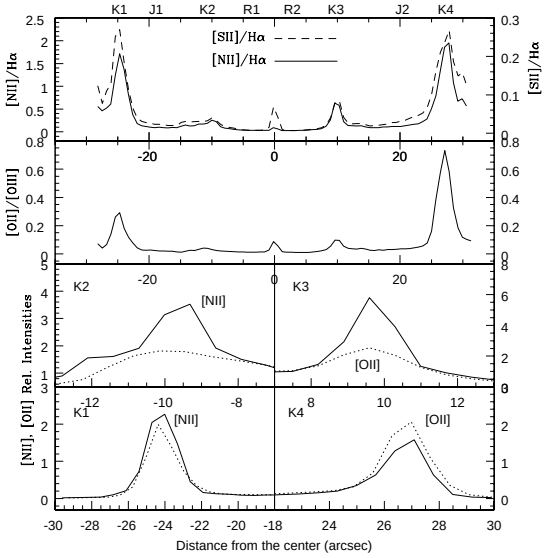

Fig. 3.— Emission line spatial distribution along P.A. = 79°. From top to bottom: the [N II]/Hα (continuous) and [S II]/Hα (dashed) line ratios; the [O II]/[O III] line ratio; the [N II] and [O II] line profiles for the inner (K_2, K_3) and outer (K_1, K_4) pairs of knots. The position of all the selected features of Figure 1 are marked at the upper part of the plot.

Concerning the general excitation structure of NGC 7009, the low-ionization ([O I], [N II], [S II], [O II]) line emission has local maxima at the position of the pairs of knots (K_{1-4}). The higher ([O III], [Ne III]) ionization emission lines, however, are much more prominent within the rim of the nebula.

As the line ratio profiles might provide additional interesting information about the excitation conditions of a nebula, we show in Figure 3 the [N II]/Hα, [S II]/Hα, [O II]/[O III], and [N II], [O II] spatial profiles along the major axis of the nebula. The top panel clearly shows the inner and outer pairs of knots as prominent zones of low ionization. Moreover, the fact that [N II]/Hα, [S II]/Hα and [O II]/[O III] ratios are very similar in shape suggests that their local maxima might not be due to the overabundance of a given element. These

line ratios are rather low at the position of the jets and the rim implying that the excitation of the jets is quite different from that of the knots. The average values of [N II]/Hα in the outer knots are 1.00 (K_1) and 0.96 (K_4), much higher than those usually found for spherical and elliptical PNe (e.g., Aller & Liller 1968). The inner pair of knots, on the other hand, have less extreme [N II]/Hα line ratios, namely 0.13 and 0.14 for K_2 and K_3, respectively.

The lower two panels of Figure 3 show the [N II] and [O II] spatial profiles at the position of the inner (top) and outer (bottom) pairs of knots. The [N II] and [O II] profiles have been normalized in the nebular regions just ahead of the knots in order to see whether the variation of the [N II] and [O II] emission through the knots shows any effects related to collisional quenching of the emission lines. The critical density for collisional de-excitation is 16 000 cm^{-3} and 3 100 cm^{-3} for the [O II] 3726 Å 3729 Å doublet, respectively, while it is 86 000 cm^{-3} for the [N II] 6583 Å line. Figure 3 shows that the [N II] and [O II] profiles are very similar in the outer, lower density ($N_e \leq 2000$ cm^{-3}) knots, whereas in both inner knots ($N_e \approx 5000$ cm^{-3}) on the contrary, the [O II] profile is much flatter than the [N II] one. This represents a direct proof that collisional quenching is indeed affecting the [O II] doublet in regions of relatively high densities, and caution should be exercised when, for example, computing densities using the [O II] doublet.

Peculiar line ratios from structures like the knots of NGC 7009 have been attributed to anomalous abundances and/or shock excitation (Balick et al. 1987; Miranda & Solf 1992). In order to test whether shock excitation plays a role in NGC 7009, we show in Figure 4 two relevant diagnostic diagrams (c.f. Cantó 1981; Phillips & Cuesta 1999). The behavior of the different components of NGC 7009 in the Hα/[N II] (6548 + 6583) versus Hα/[S II] (6716 + 6731) diagram is very interesting, revealing the eight regions to be neatly separated and ordered in pairs along the PN band. This is in line with the trends found in other PNe (see the case of M 2-9, Phillips & Cuesta 1999): the rim appears on the right of the diagram, whereas the outer zones of the nebula lie in the bottom left of the diagram. An interesting result from this diagram is that the jets and

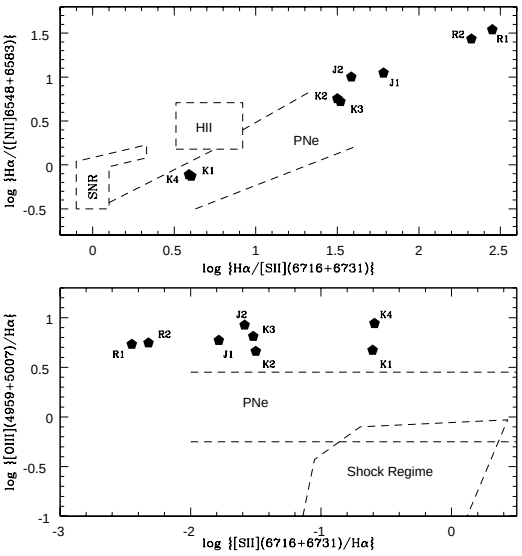

Fig. 4.— Diagnostic diagrams showing the loci of the different observed structures in NGC 7009: *Top*, log Hα/[N II](6548 + 6583) versus log Hα/[S II](6716 + 6731), from Cantó (1981). *Bottom*, log [O III](4959 + 5007)/Hα versus log [S II](6716+6731)/Hα from Phillips & Cuesta (1999).

rim, which are high-excitation zones are on the right side, while both pairs of knots appear to be separated from the former in terms of degree of excitation.

The bottom panel of Figure 4, showing [O III](4959 + 5007)/Hα versus [S II](6716 + 6731)/Hα, separates the zone of radiatively excited emission lines (the PN zone, adapted from Phillips & Cuesta 1999) from the zone mainly excited by shocks (from the predictions of the plane–parallel and bow-shock models of Hartigan, Raymond, & Hartmann 1987). It is clear that all eight structures in NGC 7009 are mainly radiatively excited by the PN central star. This is remarkable, since other PNe show, at least in some of their morphological components, indications of shock excitation, whereas in NGC 7009 not even the jet and outer knots approach the shock area in Figure 4. On the other hand, the fact that forbidden lines are radiatively excited in this nebula validates our calculations of physico-chemical parameters for the different regions.

4.4. Chemical Abundances

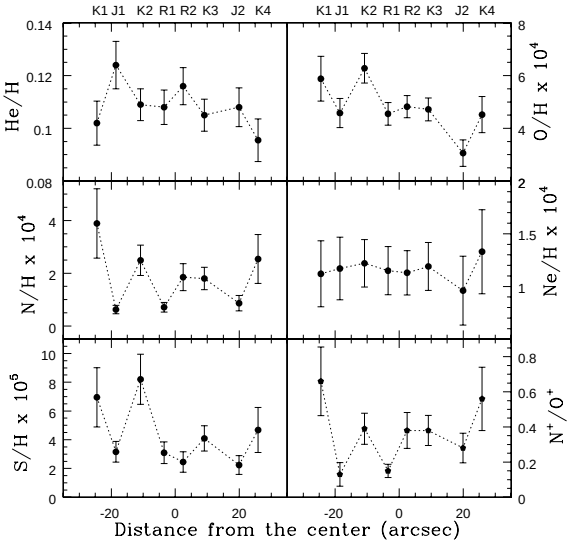

Fig. 5.— Total abundances profiles for He, O, N, Ne and S. The bottom-right panel shows the N^+/O^+ profile. The position of all the features selected from Figure 1 are marked in the upper part of the plot.

The chemical composition of a PN results from the mixing of the elements produced by the central star and dredged up to the surface with those present in the original gas from which the star was made. The abundances of O, Ne, Ar, and S are thought to represent the chemical composition of the interstellar medium when the progenitor star was born, since these elements are neither produced by the PN progenitor nor very much affected by nucleosynthesis (see Iben & Renzini 1983 and Stasińska 2002 for reviews). On the contrary, He, C, and N changes dramatically in the progenitor star enriching the stellar surface and, owing to the dredge-up episodes, enrich the PN envelopes.

Abundances of ionized nebulae are calculated based either on empirical methods or on model fitting (Stasińska 2002). In the former case, complete multiwavelength data would give the emission for all ions of a given element, and the total abundance is the sum of the ionic ones. Usually, however, only a few lines of some ions can be measured and one must correct for unseen ions using ionization correction factors.

Here, we have computed the ionic and total abundances (relative to hydrogen) for the different regions of NGC 7009, and also for the whole nebula via the ionization correction factors (*icf*) following the scheme in Kingsburgh & Barlow (1994), as done, for example, by Corradi et al. (1997). The uncertainties in this method have been discussed by Alexander & Balick (1997) and appear to be significant for the analysis of spatially resolved long-slit observations.

Table 3 lists the ionic and total abundances and the *icf* used. Total abundance profiles along the major axis of the nebula are shown in Figure 5. Errors in the ionic abundances are derived by taking into account both the errors in the line ratios and those in the adopted temperatures. Errors in the total abundances are obtained by propagating the errors in the ionic abundances as well as on the *icf*. Typical resulting errors (1σ) in the total abundances are less than 10% for He (for which no *icf* is applied), 10–20% for O, less than 35% for Ne, and 25–40% for N and S.

First of all note in Figure 5 that the abundances obtained for the regions J_1 and J_2 should be interpreted with great caution because these are indeed very faint regions in the nebula. In particular, the [N II] λ5755 Å line could not be measured at the jet positions, and we could not determine T_e[N II]. Instead, we have assumed T_e[N II] = T_e[O III] for J_1 and J_2, based on the fact that the T_e[N II] to T_e[O III] ratio of all the other regions ranges between 1.01 and 1.25. Therefore, although the adopted temperature for J_1 and J_2 seems reasonable, the ionic abundances of the low-ionization ions for these regions are probably more uncertain than the quoted errors.

Figure 5 shows that the abundance of Neon remains constant throughout the nebula. Oxygen and Sulfur abundances appear larger in K_1 and K_2 than in the other regions, but the variations are under the 2σ level. The constancy of these elements is expected from stellar evolution theory and is consistent with previous results for most spatially resolved PNe studied so far (cf. Perinotto & Corradi 1998). Helium also remains practically constant, implying no or little enrichment in the nebular ejecta.

Figure 5 also shows evidence for an increase of the N abundance in the outer knots K_1 and K_4, as previously suggested by Balick et al. (1994). They

reported a much higher overabundance, up to a factor of 5 for both K_4 and K_3 (their western ansa and cap), although they also warned that their uncertainties in the abundances could be as high as a factor of 2.

Our results can also be compared with those of other authors, who found "peculiar" abundances of N and O for certain zones of NGC 7009. An overabundance of N/H in the outer knots of a factor of 2 or more with respect to the other regions of the nebula was first derived by Czyzak & Aller (1979). Baker (1983), on the other hand, found that the N abundance does not vary substantially through the PN, but that O/H is marginally (by a factor of ~ 2) lower at the position of the outer knots. Note, however, that based on much better data and an analysis of four PNe containing ansae and including NGC 7009, Balick et al. (1994) concluded that *only* N/H increases at the ansae, by a factor between 2 and 5 as compared with the rim. Such behavior was interpreted as the result of the recent ejection of N-enriched high-velocity material by the PN central star.

A good test to investigate further this point is the inspection of the profile of the N^+/O^+ ionic abundance ratio (commonly taken as a measure of the total N/O abundance that does not depend on *icf* corrections). This is shown in the bottom right panel of Figure 5, and shows the same trend as the N/H ratio. N/O ratios deduced by Czyzak & Aller (1979) also show an apparent gradient from the rim to the ansae. Note, however, that Perinotto & Corradi (1998) and Hajian et al. (1997) did not find any evidence of peculiar N or O abundances in the 17 PNe studied, some of which possess ansae.

Finally, our total abundances of He, O, N, Ne, and S for the whole nebula (integrated over the entire slit, i.e. those labeled NEB in Table 3) are in a general agreement with those obtained by Baker (1983), Liu et al. (1995), and Hyung & Aller (1995). More accurate abundances were derived by Pottasch (2000) combining IUE and ISO/IRAS line fluxes with optical data from the literature, and are also listed in Table 3. These abundances have *icf* of order of unity and it is therefore relevant to compare them with our values. Percentual differences (from 4% for He to 30-40% for N and Ne) are similar to our estimated errors and indicate a fair level of agreement between the two sets.

We find that the sulfur abundance for the whole nebula is lower than the corresponding solar value, while the He, O and Ne ones are approximately solar (Grevesse & Anders 1989; Allende-Prieto et al. 2001); the N abundance appears similar or marginally higher than the solar value.

In conclusion, we find a homogeneous elemental abundance across the nebula, to within 9%, 17%, and 35% for He, O, Ne and S, respectively. Nitrogen seems to be enhanced in the outermost knots of NGC 7009 by a factor $\lesssim 2$, but this evidence is only marginal considering the errors and the enormous range in the derived *icf*. The uncertainties intrinsic to the method are also rather large (Alexander & Balick 1997), but the present data seem to discard variations at the level found by Balick et al. (1994).

5. Discussions

How the observed physico-chemical characteristics of the microstructures in NGC 7009 fit into current models for LIS formation and evolution? Let us first note that discrete knots such as K_1 to K_4 could form during the evolution of continuous jets: dense knots develop at the tips of jets as matter accumulates at the head of the jet, while knots in the main body of the jet can originate via several forms of instabilities (kink, Vishniac, Rayleigh–Taylor, and Kelvin–Helmholtz). Sometimes, both jets and knots are observed, whereas in other instances we observe only the latter. From a theoretical point of view, the cooling conditions on the post-shock gas and the stage of the jet's evolution mainly determine whether or not both jets and knots are seen (see, for instance, Soker 1990; Frank, Balick & Livio 1996 and García-Segura 1997).

According to hydrodynamical (HD) and magnetohydrodynamical (MHD) studies (García-Segura et al. 1999; García-Segura & López 2000; Steffen, López, & Lim 2001; Gardiner & Frank 2001; Blackman et al. 2001), the interplay between the stellar AGB and post-AGB winds (for single-star progenitors) or between stellar and disk winds (if the progenitor is a binary star) can form highly collimated jets in PNe. Jets that originate in this way are supersonic, highly collimated, two-sided, and roughly coeval with the main shell (single star) or younger (binaries). Another characteristic of some of the models is the linear increase

of the jets' expansion velocity with distance from the center (García-Segura et al. 1999; Steffen et al. 2001). The orientation of jets that result from these models depends on the alignment between the shell axis and the disk/rotation (or magnetic) axis (García-Segura & López 2000; Blackman et al. 2001), as well as on the presence of precession or wobbling (Cliffe et al. 1995; García-Segura 1997; Livio & Pringle 1997).

If the kinematical results of Reay & Atherton (1985) are correct (but see the discussion in Section 3), then, as we have shown in a previous paper (Gonçalves et al. 2001), the morphology and kinematics of the jet and knots of NCG 7009 can be qualitatively explained in the light of HD or MHD single-star interacting stellar wind model. However, as far as the comparison of our results with models in terms of physical parameters is concerned, the situation becomes worse. On the one hand, most of the above models do not show clear predictions for the densities and temperatures of jets and knots. On the other hand, those which do show such predictions are hardly in agreement with the physical parameters derived from the present observations, as we will show in the following.

The simple process of mass accumulation implies that knots at the jets' tips are necessarily denser than the jets themselves. As we showed in Section 4 this is not the case in NGC 7009. An additional, very intriguing, property of the jets/knots of this PN is that we find no evidence for shock excitation from the optical lines (the line ratios of the jets and outer knots appear to be essentially radiatively excited, see Section 4.3).

Further insights can be gained by comparing our results with the following detailed models. Steffen et al. (2001) developed HD stagnation knot/jet 2-D models which are based on the slow AGB and fast post-AGB winds interaction with lack of momentum in the polar direction of the main shell. They show that this interaction gives rise to "microstructures" which first produce a slightly elongated knot attached to the rim, then a knot further elongated and detached to the rim, and finally a polar jet with a characteristic outward linear increase in velocity. The stagnation knot/jet model has transient lower density jets with higher density knots at the tips, but the opposite occurs with the more permanent jet structures. Therefore, the stagnation knot/jet models do not explain the outer knots and jets of NGC 7009, whose outer pair of knots and jets have very similar densities, contrary to the model predictions.

Recent 3D MHD models by García-Segura & López (2000) can also be qualitatively compared with our results. These models seem to be able to reproduce successfully the formation of large- and small-scale structures in PNe. These authors state that the mass-loss rate during the post-AGB is a key parameter in distinguishing between the formation of PNe with highly collimated jets and PNe with knots (ansae-like structures): $\dot{M} \gtrsim 10^{-7}\ M_{\odot}\ \mathrm{yr}^{-1}$ leads to the formation of jets, while lower mass-loss rates ($\dot{M} \sim 10^{-8}\ M_{\odot}\ \mathrm{yr}^{-1}$) are only able to produce knots, instead of jets. Although the low resolution of these models precludes making quantitative predictions for the physical parameters of the knots and jets, their results suggest (their Figure 7) that jets and knots are indeed shock-dominated while our analysis indicates that the jets and the outer knots of NGC 7009 are mainly radiatively excited.

An alternative possibility for the formation of polar knots/jets in elliptical PNe is the model proposed by Frank et al. (1996). They suggest that jets and ansae can be formed during the "momentum-conserving" proto-PN stage, i.e., before the beginning of the fast wind. The key ingredients of this model are the gradual change from a slow to a fast wind, as well as an appreciable equator-to-pole density contrast in the slow wind. The accelerated wind would flow preferentially parallel to the shock, and the gas would follow the shocks' prolate boundary toward the polar axis. The final result is that the gas flows converge at the polar axis where they collide, form a new shock that redirects the flow into a jet, and moves outward along the main axis of the bubble. Jets/ansae formed this way can be accelerated up to $70\,\mathrm{km\,s^{-1}}$ and have densities $> 10^6\ \mathrm{cm}^{-3}$, before being ionized by the UV photons of the post-AGB star.

In fact the jet/ansae of NGC 7009 look like a continuity of its elliptical rim (remembering that rim and jet are very similar in excitation degree), which is very much in the line of the "converging polar flows" model for the formation of jets and ansae. However, such flows do not tend

to converge into stable "microstructures", since the fast/slow wind interaction could destroy these structures (Frank et al. 1996; Dwarkadas & Balick 1998; López 2002).

Finally, if the nitrogen overabundance of the outer pair of knots is taken as real (but see the discussion in Section 4.4), the formation of K_1 and K_4 might be related to recent high-velocity ejections of enriched material from the central star. Such a conclusion requires that the high-velocity nature of the structures is effectively confirmed by more robust kinematical data (especially concerning the proper motions).

Another issue to be further investigated is the relation between the thin jet and the "fat" polar bubbles of the nebular shell. The jet seems to be located along the polar axis of the bubbles, and the outer knots lie exactly at the edge of the bubbles. It is then conceivable that the outer knots are the results of the interaction of the jet with the walls of the bubbles. However, would such interaction enhance the low-ionization emission without developing a significant density contrast, as observed?

The formation of the inner system of knots is also uncertain. Morphologically, the knots seem to be located in the shell, and might well share its expansion velocity, as found in other PNe, such as IC 2553 and NGC 5882 (Corradi et al. 2000). If so, they could well be the results of in situ instabilities, or survivors of pre-existing condensations in the AGB wind. Our suggestions for the formation of the outer and inner pair of knots can readily be tested with adequate kinematical modeling of the different structures in NGC 7009.

6. Conclusions

A physico-chemical investigation of the symmetrical pairs of structures – rim, inner and outer knots, and jetlike systems connecting the latter – in NGC 7009 is presented. This study, the most extensive (eight individual regions along the major axis), better resolved (1 arcsec spatial resolution within the central 1 arcmin) and complete to date (including all diagnosis from available optical lines), has revealed a clear and coherent pattern of physical, excitation, and chemical characteristics through the nebula: 1) the electron temperature, both for low- and high- excitation species, is remarkably constant; 2) electron densities are similar for both the jetlike structures and the outer knots, but they are roughly one-third of those found in the pair of inner knots and the rim; 3) no sign of shock excitation is found for any of the microstructures or the rim; and 4) a notable chemical uniformity is found for the eight regions studied, with the exception of a marginal, moderate ($\times$ 2) enhancement of nitrogen at the outernmost knots.

The origin of the system of microstructures in NGC 7009 is discussed in the light of its physico-chemical parameters and the available theoretical models, but none of these appears able to account for both the lack of a strong density contrast between the outer knots and jetlike structures, and the absence of shocks in them. More than 200 years after its discovery by Herschel, the Saturn Nebula is still challenging our comprehension.

7. Acknowledgments

We would like to thank the referee, Letizia Stanghellini, for several useful comments and suggestions that had help us to improve the paper. We are grateful to F. Sabbadin for detecting a misidentification (now corrected) of features in Fig. 1 of the preprint. The work of DRG, RLMC and AM is partially supported by a grant from the Spanish Ministry of Science and Technology (AYA 2001-1646).

REFERENCES

Acker, A., Ochsenbein, F., Stenholm, B., Tylenda, R., Marcout, J., & Schohn, C., 1992, Strasbourg-ESO catalogue of Galactic planetary nebulae, ESO

Alexander, J., & Balick, B. 1997, AJ, 114, 713

Allende-Prieto, C., Lambert, D. L., & Asplund, M. 2001, ApJ, 556, 63

Aller, L. H., & Liller, W. 1968, in Nebulae and Interstellar Matter, ed. B. M. Middlehurst & Aller (Chicago: Univ. Press), 498

Baker, T. 1983, ApJ, 267, 630

Balick, B. 1987, AJ, 94, 671

Balick, B., Alexander, J., Hajian, A. R., Terzian, Y., Perinotto, M., & Patriarchi, P. 1998, AJ, 116, 360

Balick, B., Owen, R., Bignell, C. R., & Hjellming, R. M. 1987, AJ, 94, 948

Balick, B., Perinotto, M., Maccioni, A., Alexander, Terzian, Y., & Hajian, A. R. 1994, ApJ, 424, 800

Balick B., Preston, H. L, & Icke, V. 1987, AJ, 94, 164

Balick B., Rugers, M., Terzian, Y., & Chengalur, J. N. 1993, ApJ, 411, 778

Blackman, E. G., Frank, A., & Welch, C. 2001, ApJ, 546, 288

Bohigas, J., López, J. A., & Aguilar, L. 1994, A&A, 291, 595

Cahn, J. H., Kaler, J. B., & Stanghellini, L. 1992, A&AS, 94, 399

Cardelli, J. A., Clayton, G. C., & Mathis, J. S. 1989, ApJ, 345, 245

Cantó, J. 1981, In: Investigating the universe, by D. Reidel Publishing Co., p. 95

Cliffe, J. A., Frank, A., & Livio, M., Jones, T. W. 1995, ApJ, 447, L49

Copetti, M. V. F., & Writzl, B. C. 2002, A&A, 382, 282

Corradi, R. L. M., Manso, R., Mampaso, A., & Schwarz, H. E. 1996, A&A, 313, 913

Corradi, R. L. M., Gonçalves, D. R., Villaver, E., Mampaso, A., & Perinotto, M. 2000, ApJ, 542, 861

Corradi, R. L. M, Perinotto, M., Schwarz, H. E., Claeskens, J-F 1997, A&A, 322, 975

Czyzak, S. J., & Aller, L. H. 1979, MNRAS, 188, 229

Dwarkadas, V. V., & Balick, B. 1998, ApJ, 497, 267

De Robertis, M., Dufour, R. & Hunt, R. 1987, JRASC, 81, 195

Frank, A., Balick, B., & Livio, M. 1996, ApJ, 471, L53

Frank, A., & Mellema, G. 1994, ApJ, 430, 800

García-Segura, G. 1997, ApJ, 489, 189

García-Segura, G., Langer, N., Rózyczka, M., & Franco, J. 1999, ApJ, 517, 767

García-Segura, G., & López, J. A. 2000, ApJ, 544, 336

Gardiner, T. A., & Frank, A. 2001, ApJ, 557, 250

Gonçalves, D. R., Corradi, R. L. M., & Mampaso, A. 2001, ApJ, 547, 302

Górny, S. K., Schwarz, H. E., Corradi, R. L. M., & van Winckel, H. 1999, A&AS, 136, 145

Grevesse, N., & anders, E. 1989, in Waddington J., ed., Cosmic Abundances in Matter, AIP, New York, p. 1

Guerrero, M. A., Gruendl, R. A., & Chu, Y.-H. 200 2, A&A, 387, L1

Hajian, A. R., Balick, B., Terzian, Y., & Perinotto, M. 1997, ApJ, 487, 313

Hartigan, P., Raymond, J., & Hartmann, L. 1987, ApJ, 316, 323

Hyung, S., & Aller, L. H. 1995, MNRAS, 273, 958

Iben, I, & Renzini, A. 1983, ARA&A, 21, 271

Kingsburgh, R. L., & Barlow, M. J. 1992, MNRAS, 257, 317

Kingsburgh, R. L., & Barlow, M. J. 1994, MNRAS, 271, 257

Kwok, S., Purton, C. R., Fitzgerald, P.M. 1978, ApJ, 219, L125

Lame, N. J., & Pogge, R. W. 1996, AJ, 111, 2320

Liller, W. 1965, PASP, 77, 25

Liu, X.-W., Storey, P. J., Barlow, M. J., Clegg, R. E. S. 1995, MNRAS, 272, 369

Livio, M. & Pringle, J. E. 1997, ApJ, 486, 835

López, J. A., Vázquez, R., & Rodríguez, L. F. 1995, ApJ, 455, L63

López, J. A. 1997, in Planetary Nebulae, Proccedings of the 180th Symposium of the IAU, ed. H. J. Habing. and H. J. G. L. Lamers. Publisher: Dordrecht Kluwer Academic Publ., p. 197

López, J. A. 2002, in "Emission Lines from Jet Flows", Eds. W.J. Henney, W. Steffen, A.C. Raga & L. Binette, RevMexAA (Conference Series), 13, p. 139

Maciel, W. J. 1995, Ap&SS, 229, 203

Manchado, A., Guerrero, M. A., Stanghellini, L., & Serra-Ricart, M. 1996, The IAC Morphological Catalog of Northern Galactic PNe, IAC Publ.

Mellema, G., & Frank, A. 1995, MNRAS, 273, 401

Méndez, R. H., Kudritzki, R. P., & Herrero, A. 1992, A&A, 260, 329

Miranda, L. F., & Solf, J. 1992, A&A, 260, 397

Osterbrock, D. E., 1989, "Astrophysics of Gaseous Nebulae and Active Galctive Nuclei". University Science Books, ed. Mill Valey, California.

Perinotto, M. & Corradi, R. M. L. 1998, A&A, 332, 721

Phillips, J. P., & Cueta, L. 1999, AJ, 118, 2919

Pottasch, S. R. 2000, in Asymmetrical Planetary Nebulae II: From Origins to Microstructures, ASP Conference Series, Vol. 199., Edited by J. H. Kastner, N. Soker, and S. Rappaport, p. 289

Reay, N. K., & Atherton, P.D. 1985, MNRAS, 215, 233

Rubin, R. H., et al. 2002, MNRAS, 334, 777

Shaw, R. A., & Dufour, R. J. 1995, PASP, 107, 896

Schwarz, H. E., Corradi, R. L. M., & Melnick, J. 1992, A&AS, 96, 23

Schönberner, D. 2002, in "Planetary Nebulae and Their Role in the Universe", proceedings of IAU Symposium No. 209, ASP Conference Series

Soker, N. 1990, AJ, 99, 1869

Stasińska, G. 2002, to be published in the proceedings of the XIII Canary Islands Winter School of Astrophysics (astro-ph/0207500)

Steffen, W., López, J. A., & Lim, A. 2001, ApJ, 556, 823

Zhang, C. Y., & Kwok, S. 1998, ApJS, 117, 341

This 2-column preprint was prepared with the AAS LaTeX macros v5.0.

Table 1

Measured line fluxes normalized to Hβ=100.

Line identification	K_1	J_1	K_2	R_1	R_2	K_3	J_2	K_4	NEB
[OII] 3726.0 + 3728.8	182	63.5	27.3	13.8	6.52	24.8	27.0	138	21.5
H12 3750.15	-	1.87	1.28	2.12	1.64	2.05	3.53	1.72	2.05
H11 3770.6	2.14	3.25	1.65	2.31	2.10	2.53	3.95	2.35	2.48
H10 3797.9	2.07	3.37	2.77	3.67	3.05	3.68	5.52	3.49	3.69
H9 3835.4	3.08	7.90	4.49	6.01	5.40	6.21	10.2	7.35	6.10
[NeIII] 3868.7	74.0	114	74.2	95.5	94.4	99.4	150	127	97.1
HeI 3888.7 + H8 3889.1	12.9	25.9	15.4	20.0	14.6	19.3	32.2	22.6	18.8
[NeIII] 3967.5 + Hϵ 3970.1	32.0	53.5	36.2	46.9	40.5	46.1	70.5	54.2	44.4
HeI 4026.0	1.70	2.94	1.90	2.32	2.00	2.35	3.78	2.66	2.23
[SII] 4068.6	6.81	3.20	1.71	1.38	2.17	2.15	2.63	4.62	1.82
[SII] 4076.4	2.17	1.53	0.78	0.80	1.07	0.98	0.84	1.68	1.02
Hδ 4101.8	14.9	30.0	21.0	28.0	22.3	28.0	40.5	27.8	27.0
HeI 4120.	-	-	-	0.49	-	-	-	-	0.52
OII + HeI 4143.7	-	-	0.28	0.41	-	-	-	-	0.41
[FeV] 4228.	-	-	-	0.26	-	0.31	-	-	-
CII 4267.2	-	-	0.30	0.64	0.76	0.68	0.47	-	0.59
Hγ 4340.5	29.2	56.1	37.9	48.1	40.5	48.5	67.2	48.5	46.8
[OIII] 4363.2	6.57	9.40	5.98	7.35	8.19	7.78	13.0	9.13	7.72
HeI 4387.9	-	-	0.65	0.64	-	0.55	-	-	0.65
HeI 4471.5	3.71	6.07	4.20	5.01	4.27	5.11	7.57	5.84	4.85
HeII 4541.7	-	-	0.19	0.45	-	-	-	-	0.35
NIII + OII 4641.0	-	1.50	-	3.07	4.61	2.68	1.99	-	3.09
CIII 4647.1	-	1.28	0.59	1.13	-	0.92	1.33	-	1.04
HeII 4685.7	0.99	2.62	10.2	25.6	23.0	8.42	2.16	1.21	15.6
[ArIV] + HeI 4711+13	2.16	4.62	3.23	5.40	4.89	2.78	5.08	1.97	4.04
[ArIV] 4740.2	1.13	3.63	2.78	5.50	4.49	2.54	3.95	1.48	3.88
Hβ 4861.3	100	100	100	100	100	100	100	100	100
[OIII] 4958.9	428	473	435	405	428	424	458	454	421
[OIII] 5006.86	1256	1339	1268	1179	1243	1227	1381	1329	1223
[ArIII] 5191.8	-	-	0.09	-	-	-	-	-	0.07
[NI] 5200.2	6.06	-	0.06	-	-	-	-	2.82	0.11
[FeIII] 5270.	-	-	-	-	-	-	-	-	0.08

TABLE 1—*Continued*

Line identification	K_1	J_1	K_2	R_1	R_2	K_3	J_2	K_4	NEB
[FeIII] + [CaV 5292.	-	-	-	-	-	-	-	-	0.09
HeII 5411.6	-	-	0.72	1.48	1.67	0.95	-	-	1.12
[ClIII] 5517.7	-	-	0.71	0.46	0.46	0.55	0.91	1.03	0.58
[ClIII] 5537.9	-	0.40	0.85	0.57	0.59	0.71	0.79	0.96	0.68
[OI] 5577.4	0.51	-	0.14	-	-	-	-	-	0.01
[OIII] 5592.4	-	-	-	0.03	0.40	-	-	-	0.05
[NII] 5754.6	6.95	-	0.72	0.15	0.20	0.69	-	4.19	0.50
HeI 5875.7	20.3	17.0	17.9	15.0	15.3	15.8	15.8	16.2	15.7
[KIV] 6102.	-	-	-	0.16	0.18	0.11	-	-	0.15
HeII 6166 + 6170	-	-	-	-	-	-	-	-	0.06
HeII 6234.	-	-	-	-	-	-	-	-	0.06
[OI] 6300.3	31.0	-	1.02	-	-	1.69	-	14.8	1.06
[SIII] 6312.1	4.29	1.80	2.84	1.41	1.26	1.97	1.50	3.59	1.86
SiII 6347.1	-	-	-	0.07	-	-	-	-	-
[OI] 6363.8	11.3	-	0.38	0.12	0.17	0.56	-	5.33	0.36
SiII 6371.	-	-	-	0.10	0.12	-	-	-	-
HeII 6406.5	-	-	-	0.19	0.19	-	-	-	-
[NII] 6548.0	132	10.8	17.9	3.57	3.57	13.9	7.05	72.5	11.2
Hα 6562.8	394	337	408	312	341	280	217	224	313
[NII] 6583.4	397	19.5	53.8	7.93	6.26	39.2	14.7	217	30.2
HeI 6678.1	8.41	5.52	6.16	4.35	4.44	4.00	3.74	3.57	4.46
[SII] 6716.5	41.4	2.52	4.82	0.54	0.43	3.13	2.59	26.1	2.63
[SII] 6730.8	57.4	3.09	8.19	0.95	0.78	5.42	3.05	32.0	4.34
N_e[S II]	2000	1300	4500	5500	5900	5000	1100	1300	4000
N_e[Cl III]	-	-	4700	5200	5900	6000	1300	1900	4500
T_e[O III]	9600	10 400	9300	10 000	10 200	10 100	11 600	10 400	10 100
T_e[N II]	11 000	-	9400	10 400	12 800	10 400	-	11 700	10 300
T_e[S II]	7100	-	8300	-	-	-	-	9400	-

TABLE 2

ESTIMATED PERCENTAGE ERRORS IN LINE FLUXES IN TABLE 1 AND Hβ FLUXES

Line fluxes	K_1 4.9[a]	J_1 4.2[a]	K_2 8.4[a]	R_1 3.5[a]	R_2 1.4[a]	K_3 9.1[a]	J_2 4.9[a]	K_4 4.9[a]	NEB 55.3[a]
(0.01–0.05)$I_{H\beta}$	26	31	5	6	10	4.5	11	13.5	4
(0.05–0.15)$I_{H\beta}$	14	10	3.5	4	6.5	3.5	7.5	10	3.5
(0.15–0.30)$I_{H\beta}$	9	8	3.5	3.5	4.5	3.5	6	7.5	3
(0.30–2.0)$I_{H\beta}$	6	6	3.5	3.5	3.5	3	4.5	5.5	3
(2.0–5.0)$I_{H\beta}$	5	4.5	3	3.5	3.5	3	4	5	3
(5.0–10.0)$I_{H\beta}$	4.5	4	3	3	3	3	4	5	3
> 10 $I_{H\beta}$	4	4	3	3	3	3	4	5	3
$I_{H\beta}$[b]	1.05(6)	1.24(6)	30.2(4)	30.7(4)	15.5(4)	70.2(3)	1.60(5)	1.28(6)	188(3)

[a]Size (in arcsec) of the selected structure along the slit.

[b]In units of 10^{-13} erg cm^{-2} s^{-1}. Values within brackets are the estimated percentage errors in the Hβ line emission.

TABLE 3

IONIC/TOTAL ABUNDANCES[1]

	K_1	J_1	K_2	R_1	R_2	K_3	J_2	K_4	NEB	NEB - Pottasch
He^+/H	1.02E-1(06)	1.23E-1(05)	1.04E-1(04)	9.54E-2(04)	9.18E-2(04)	9.46E-2(04)	1.07E-1(05)	9.55E-2(06)	9.77E-2(04)	
He^{2+}/H	-	1.2E-3(10)	5.02E-3(06)	1.24E-2(07)	2.43E-2(06)	1.07E-2(07)	1.87E-3(08)	-	1.30E-2(06)	
He/H	**1.02E-1(09)**	**1.24E-1(08)**	**1.09E-1(06)**	**1.08E-1(08)**	**1.16E-1(06)**	**1.05E-1(06)**	**1.08E-1(08)**	**9.55E-2(09)**	**1.11E-1(06)**	**1.107E-1**
O^0/H	4.5E-5(11)	-	2.40E-6(09)	5.0E-7(13)	3.1E-7(16)	2.61E-6(08)	-	1.8E-5(13)	1.71E-6(08)	
O^+/H	7.5E-5(19)	2.2E-5(13)	2.4E-5(14)	7.0E-6(15)	1.3E-6(16)	1.4E-5(14)	6.06E-6(17)	4.2E-5(21)	1.2E-5(13)	
O^{2+}/H	5.12E-4(09)	4.32E-4(08)	5.84E-4(06)	4.12E-4(07)	4.11E-4(06)	4.25E-4(06)	2.9E-4(10)	4.1E-4(10)	4.21E-4(06)	
icf(O)	1.00	1.00	1.03	1.08	1.16	1.07	1.01	1.00	1.08	
O/H	**5.8E-4(15)**	**6.4E-4(12)**	**6.28E-4(09)**	**4.5E-4(11)**	**4.82E-4(09)**	**4.7E-4(11)**	**3.0E-4(15)**	**4.5E-4(17)**	**4.71E-4(09)**	**5.2E-4**
N^0/H	8.7E-6(16)	-	2.2E-7(12)	-	-	-	-	2.7E-6(19)	2.7E-7(11)	
N^+/H	5.00E-5(08)	3.09E-6(07)	9.66E-6(06)	1.10E-6(07)	5.19E-7(08)	5.59E-6(06)	1.7E-6(10)	2.38E-5(09)	4.45E-6(06)	
icf(N)	7.8	20.1	25.7	64.7	355	32.1	50.5	10.6	38.2	
N/H	**3.8E-4(35)**	**6.2E-5(26)**	**2.4E-4(24)**	**7.0E-5(26)**	**1.8E-4(29)**	**1.8E-4(24)**	**8.6E-5(34)**	**2.5E-4(38)**	**1.7E-4(23)**	**1.3E-4**
Ne^{2+}/H	9.8E-5(14)	1.1E-4(12)	1.1E-4(10)	1.0E-4(10)	9.6E-5(10)	1.0E-4(10)	9.3E-5(17)	1.2E-4(15)	1.05E-4(09)	
icf(Ne)	1.14	1.06	1.07	1.10	1.17	1.11	1.03	1.10	1.11	
Ne/H	**1.1E-4(29)**	**1.1E-4(26)**	**1.2E-4(20)**	**1.1E-4(21)**	**1.1E-4(20)**	**1.1E-4(20)**	**9.6E-5(34)**	**1.3E-4(30)**	**1.1E-4(18)**	**1.9E-4**
S^+/H	2.2E-6(13)	8.99E-8(08)	5.11E-7(08)	4.4E-8(11)	2.2E-8(13)	2.7E-7(10)	7.0E-8(10)	1.0E-6(14)	2.09E-7(06)	
S^{2+}/H	7.45E-6(21)	3.2E-6(15)	7.4E-6(14)	2.1E-6(16)	9.7E-7(19)	3.4E-6(14)	1.6E-6(19)	4.8E-6(23)	3.3E-6(13)	
icf(S)	1.43	1.91	2.07	2.79	4.91	2.22	2.58	1.57	2.35	
S/H	**1.39E-5(30)**	**6.3E-6(23)**	**1.6E-5(23)**	**6.1E-6(26)**	**4.9E-6(30)**	**8.1E-6(23)**	**4.4 E-6(29)**	**9.3E-6(35)**	**8.3E-6(26)**	**11.1E-6(26)**

[1]Estimated percentage errors in brackets.